Water Supply

IWA PUBLISHING

Water Supply Vol 22 No 4, 4320 doi: 10.2166/ws.2022.052

Experimental investigation of oxygen transfer efficiency in hydraulic jumps, plunging jets, and plunging breaking waves

Ashabul Hoque* and Anip Kumar Paul

Department of Mathematics, University of Rajshahi, Rajshahi 6205, Bangladesh
*Corresponding author. E-mail: mahoque@ru.ac.bd

ABSTRACT

The scope of the paper is to analyse the different similarities of air entrainment among the hydraulic jumps, plunging jets, and plunging breaking waves and to discuss current practices. The measured data are reexamined and scrutinised to investigate the gas exchange phenomena through an air-water interface. In particular, oxygen transfer efficiency and penetration depth by air bubbles are discussed. The calculated results highlight that the oxygen transfer efficiency is decreased with the increase of energy dissipation rate both in plunging jets and breaking waves. In contrast, it is shifted almost parallel in the case of hydraulic jumps. In addition, the aeration lengths in the hydraulic jumps and penetration depths both in plunging jets and plunging breaking waves were dependent on the jet impact velocity.

Key words: aeration efficiency, dissolved oxygen, hydraulic jump, penetration depth, plunging breaker, plunging jet

HIGHLIGHTS

- Air bubble entrainments through hydraulic jumps, plunging jets, and plunging breaking waves are studied.
- Aeration lengths in the hydraulic jump and penetration depths in the plunging jets and plunging breaking waves were determined.
- Dissolved oxygen, as well as oxygen transfer efficiency, were measured and compared among the phenomena.
- Scale effects were observed among the phenomena in terms of the oxygenation.

GRAPHICAL ABSTRACT

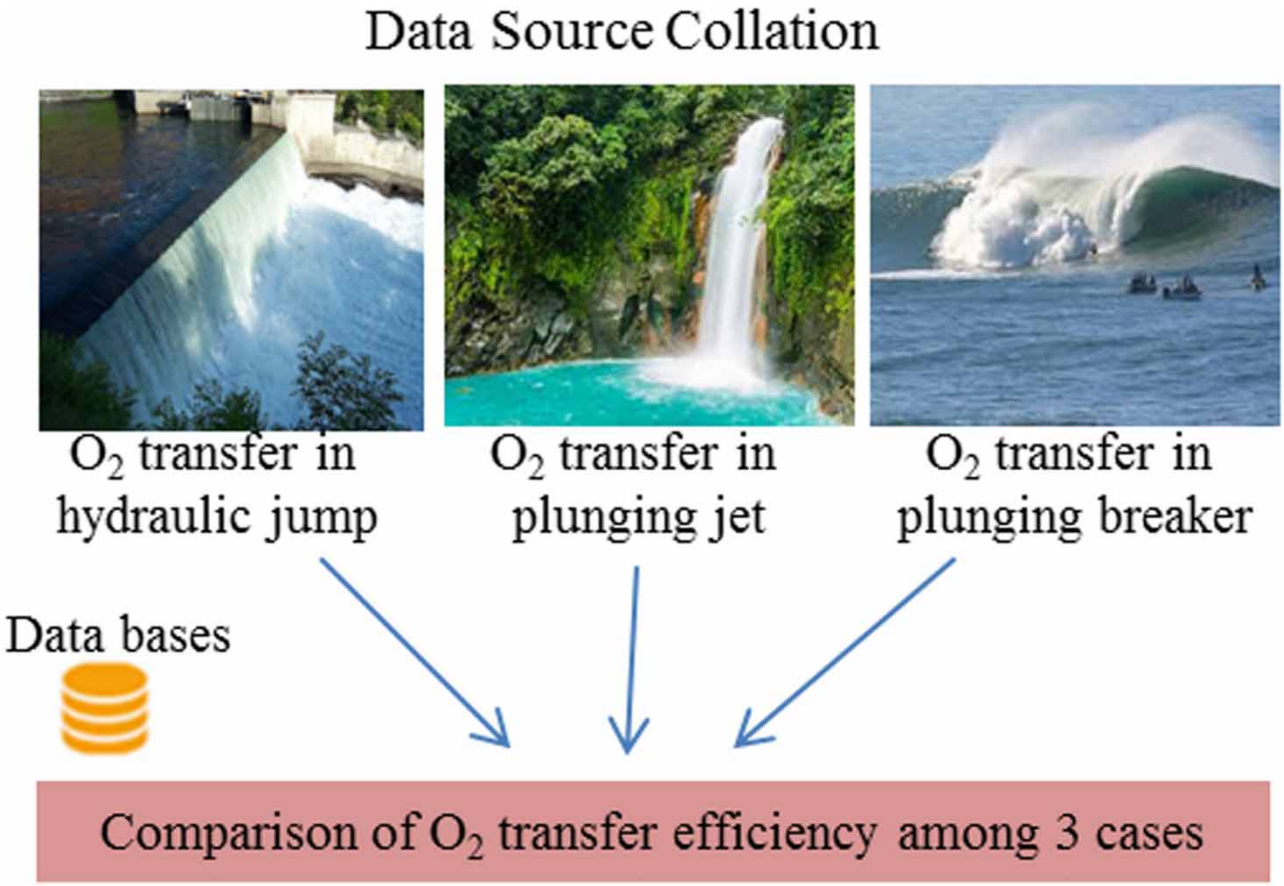

1. INTRODUCTION

Gas fluxes such as oxygen and carbon dioxide (CO_2) through the air-water interface provide significant developments of the climate system (Tans *et al.* 1990). Gas exchange occurs through air bubbles in hydraulic jumps, plunging jets, and plunging breaking waves shown in Figure 1. In nature, the CO_2 and the supersaturation of dissolved oxygen (DO; a measure of how much oxygen is dissolved in the water) in the ocean releases fresh oxygen and keep the balance among these gases in the atmosphere (Sarmiento *et al.* 1992). Arora & Keshari (2021) used machine learning techniques to predict water quality parameters, and they found that the ANFIS model worked well to predict the DO. Yang *et al.* (2021) made a novel measurement of the gas transfer efficiency based on partial equilibration of CO_2 using a segmented flow coil equilibrator system. The water is naturally pure if DO demand and supply are balanced. Anyway, if the amount of consumption of the DO exceeds the amount of collection, the water starts to degrade. Therefore, for keeping the water at the best quality, it is essential to assess the re-aeration effectiveness of water accurately.

With plunging wave breakers, the wave face forms a water jet that projects in front of the wave, and air-entraining occurs (Figure 1(c)). Plunging breaking waves generate many air bubbles, producing water turbulence. Air bubbles by breaking waves increase drastically in the surf zone for gas exchange, and they might play an important role by purifying water in the coastal area. Hosoi & Murakami (1986) found that the DO is insignificant for the non-breaking waves zone, but it was significant in the entire water body along the surf zone. Wallace & Wirick (1992) observed that the aeration rate of breaking waves could increase the entrained air bubbles up to 200 times. The numerical results obtained by Saleem *et al.* (2018) showed that the five-equation model could simulate the dynamics of the two-phase flows. Hosoi *et al.* (1984) measured the oxygen absorption in laboratory experiments during the spilling of breaking waves, and they studied the aeration efficiency related to the deep-water waves properties. Alekseyev & Kokorin (1984) measured a supersaturated DO average of 3% along with the water

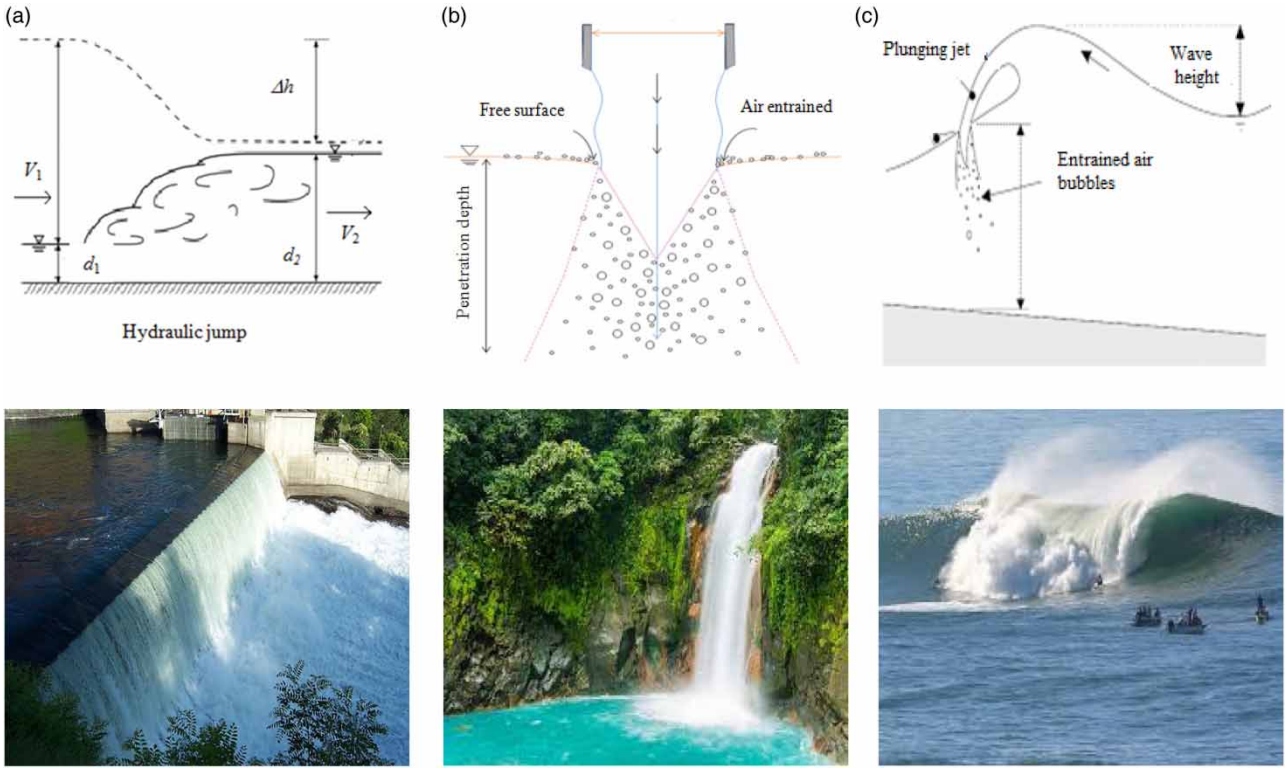

Figure 1 | Sketches and photos of air entrainment in (a) hydraulic jumps, (b) plunging jets and (c) plunging breaking waves.

depth, and this level can rise to 8% during a storm surge. But up to date, very little attention has been paid to examining the effects of gas exchange in the surf zone.

Several researchers (Van de Sande & Smith 1976; Biń 1993; Chanson 1995; Ohl *et al.* 2000; Anandraj 2012; Bostan *et al.* 2013; Harby *et al.* 2014; Jadhav *et al.* 2017; Bertola *et al.* 2018; Estrella *et al.* 2021) studied the gas exchange phenomena in plunging jets and hydraulic jumps and observed some physical characteristics of air-water flow systems made by the water jet flow. Ohl *et al.* (2000) investigated the air entrainment at the free surface of a liquid pool and showed that the crests of surface disturbances on a falling jet are a powerful agent for air entrainment. Experimental investigations for oxygen exchange by vertical plunging jets were conducted by Van de Sande & Smith (1976), and they found an empirical correlation between penetration depth and oxygen transfer rate. An experimental study by Kumar *et al.* (2018) showed a significant effect of hollow jet angle on volumetric oxygen transfer coefficient ($K_L a$) at higher jet velocities. Chanson (1995) and Chanson & Cummings (1994) developed a gas transfer model to predict the dissolved gas contents at the hydraulic jump and plunging breaking waves. Estrella *et al.* (2021) presented an extensive study of similarity and scale effects in a hydraulic jump for constant Froude number. Bertola *et al.* (2018) proposed a physical study of vertical supported planar water plunging jets in a relatively large-size facility, and results were compared favourably with the literature. Unsteady air-water flow measurements were conducted in a breaking bore propagating in a large-size channel by Leng & Chanson (2019), and they observed that air entrainment took place in the form of air entrapment at the roller toe.

On the other hand, many researchers attempted to establish relationships between aeration and energy dissipation (Chanson & Cummings 1994; Kucukali & Cokgor 2009; Bostan *et al.* 2013). Bostan *et al.* (2013) measured the dissolved oxygen in hydraulic jumps using a handy oxygen meter for five different jet flow rates. They obtained the oxygen transfer efficiency, which was increased with relative energy loss. Chanson & Cummings (1994) showed an analogy of air bubble entrainment between vertical circular plunging jets and hydraulic jumps. Wüthrich *et al.* (2020) investigated the air entrainment mechanisms for wave-breaking surge against Froude numbers. Kucukali & Cokgor (2009) measured the oxygen transfer efficiency for a hydraulic jump of unit width channel, linearly related to the energy dissipation rate. Close similarities in aeration and energy dissipation performances were found between the classical hydraulic and Type B jumps, while Type D jumps showed lower energy dissipation efficiency and aeration (Montano & Felder 2020). Cihat *et al.* (2014) indicated that

high-head gated circular conduits flow system might significantly increase the dissolution of oxygen in the water. Data-driven models were employed for estimating hydraulic jump oxygen aeration efficiency (E_{20}) under a sluice gate using experimental data and sensitivity analysis and showed that the Reynolds number was a significant parameter in the estimation of E_{20} (Tiwari 2021). Witt & Gulliver (2012) estimated the oxygen transfer coefficient from scaled formulations of the liquid film coefficient, mean bubble diameter, air entrainment rate, and turbulent energy dissipation rate. Kamal *et al.* (2020) showed that the gas transfer efficiency was high when pre-aeration (air entrainment on the spillway face) occurred. Retsinis & Papanicolaou (2020) simulated a classical hydraulic jump in a horizontal open channel, and a comparison of the numerical results with experiments showed the validity of the computations. However, up to date, none of the studies compared the oxygen transfer efficiency among the hydraulic jumps, plunging jets, and plunging wave breakers.

The penetration depth of the entrained bubbles is a significant scale in the plunging jet arrangements, which affects the size of the immersed two-phase area. The performance of the aeration system is greatly affected by the residence time of the entrained air bubbles in the case of plunging jets. Iguchi *et al.* (1998) investigated higher flow rates with the arrangement of jet-interface variability. They observed that the higher air bubbles are buoyant just below the impact point, escaping rapidly and leading to a shorter penetration. McKeogh & Ervine (1981) proposed an empirical formula of penetration depth for different setup conditions. Similar tests were conducted by Suciu & Smigelschi (1976), and they established a relationship based on measured penetration depth. Miller (1987) pointed out that the penetration depth is greater for plunging breakers than spilling breakers. Chanson (1995) measured the aeration length for the hydraulic jump, which is renamed as penetration depth for plunging jet and plunging breaker. Guyot *et al.* (2020) derived a simple mathematical expression to predict the bubble cloud penetration depth.

Thus, there is a clear need for some fundamental studies on the characterisation of air entrainment, aeration system, and oxygen transfer efficiency in hydraulic jumps, plunging jets, and plunging wave breakers. In this context, the present study presents a new series of detailed physical experiments of air entrainment in vertical plunging jets. It investigates the data of the above cases taken from several references.

More specifically, this research:

- evaluates the existing research in the proposed areas by studying basic ideas and current development towards the understanding of important controlling variables of penetration depth and aeration length;
- provides a detailed and comprehensive analysis of oxygen transfer efficiency.

2. REVIEW OF A GAS EXCHANGE MODEL

The presence of air bubbles inside the water increases the transfer of gases between the atmosphere and oceans (e.g. oxygen, carbon dioxide, nitrogen). For these gases and using Henry's and Fick's law, it is stated that an oxygen balance equation can be written as the rate of change in DO concentration (dC/dt) is proportional to the mass transfer of oxygen from the air to liquid. Mathematically, it is found as

$$\frac{dC}{dt} = K_L \frac{A}{V}[C_s - C] \tag{1}$$

where C denotes DO concentration (mg/L), C_s is the saturation concentration of DO (mg/L), A represents the area of the air-water interface (m^2), K_L is the oxygen transfer coefficient (m/s), and V is the aerated volume (m^3). Equation (1) is found by integrating within the limits $C = C_0$ and $C = C_t$; at $t = 0$ and $t = t$ as follows

$$\int_{C_0}^{C_t} \frac{dC}{C_s - C} = K_L a \int_0^t dt \tag{2}$$

which, after integration, Equation (2) becomes

$$\frac{C_s - C_0}{C_s - C_t} = \exp(K_L a t) \tag{3}$$

or

$$K_L a = \frac{1}{t} \ln\left(\frac{C_s - C_0}{C_s - C_t}\right) \tag{4}$$

where $A/V = a$ represents the surface area per unit volume, C_0 and C_t denote the oxygen concentrations at initial and at time t, respectively. Equation (4) displays that the values of $K_L a$ can be determined by the measured values of C_s, C_0, C_t, and t. An identical base of comparison of $K_L a$ is generally known as the volumetric oxygen transfer factor (Deswal & Verma 2007), which is normalised at a 20 °C standard temperature.

3. APPLICATION OF MODEL

3.1. Hydraulic jumps

Although there are many water flows, a hydraulic jump is a phenomenon in the science of hydraulics that is frequently observed in open channel flow. In a hydraulic jump, the flow is characterised by air entrainment and is the leading oxygen transfer provider. Further, it confirms the air entrainment into the water and dissipates the upstream energy. Air packets are entrapped through the impinge point, broken up into fragile air bubbles. At the hydraulic jump, air bubbles are advected downstream into the free shear layer categorised by concentrated turbulence before reaching the free surface and finally releasing to the air (Figure 1(a)).

3.1.1. Data collection

Detailed information on the experimental setup and method is published by Bostan *et al.* (2013) for hydraulic jumps. We want to briefly mention experimental conditions to determine the oxygen transfer efficiency (OTE). The tests were done in a channel with the dimensions of 0.4 m × 12 m × 0.65 m, where the side walls were made of glass. DO and water temperatures were taken manually before and after the hydraulic jump by DO200 meter for a half-minute interval. The DO meter was calibrated for each test. The experiment ranges of DO meter and temperature were 0–20 mg/L with a correctness of ±2%, and −6 to 46 °C with an accuracy of ±0.3 °C, respectively.

3.1.2. Aeration length (L_a)

Air entrainment in the hydraulic jump generates turbulence and associated energy dissipation along with the surface roller (Figure 1(a)). The roller is characterised by recirculation, containing the steaming region and the foam layer. The distance of the large-scale turbulence region is usually known as the roller length (L_r), which was derived by Hager *et al.* (1990). They re-analysed the primary data of Rajaratnam (1967) and defined the length of aeration (L_a) between impingement point and flow depth as

$$\frac{L_a}{d_2} = 3.5 * \sqrt{Fr_1 - 1.5} \tag{5}$$

where d_2 and Fr_1 denote the downstream flow depth and upstream Froude number, respectively. The aeration length advances monotonically with the increase of upstream velocity, as shown in Figure 2(a).

3.1.3. Oxygen transfer efficiency

The efficiency of oxygen transfer depends on air intake at the hydraulic jump. Gameson (1957) suggested a mathematical formula for finding oxygen transfer efficiency (OTE; aeration efficiency) as,

$$OTE = 1 - \exp(K_L a t) = \frac{C_0 - C_t}{C_s - C_t} \tag{6}$$

OTE equal to one means that the hydraulic jump has conveyed oxygen into water, where C_0 is equal to C_s. A value of OTE > 1 means that the downstream water is supersaturated which is known, namely $C_0 > C_s$, and OTE = 0 means that no oxygen transfer occurs there. Temperature plays a significant role in the mass transfer mechanism, so oxygen transfer efficiency should be transformed based on the average temperature.

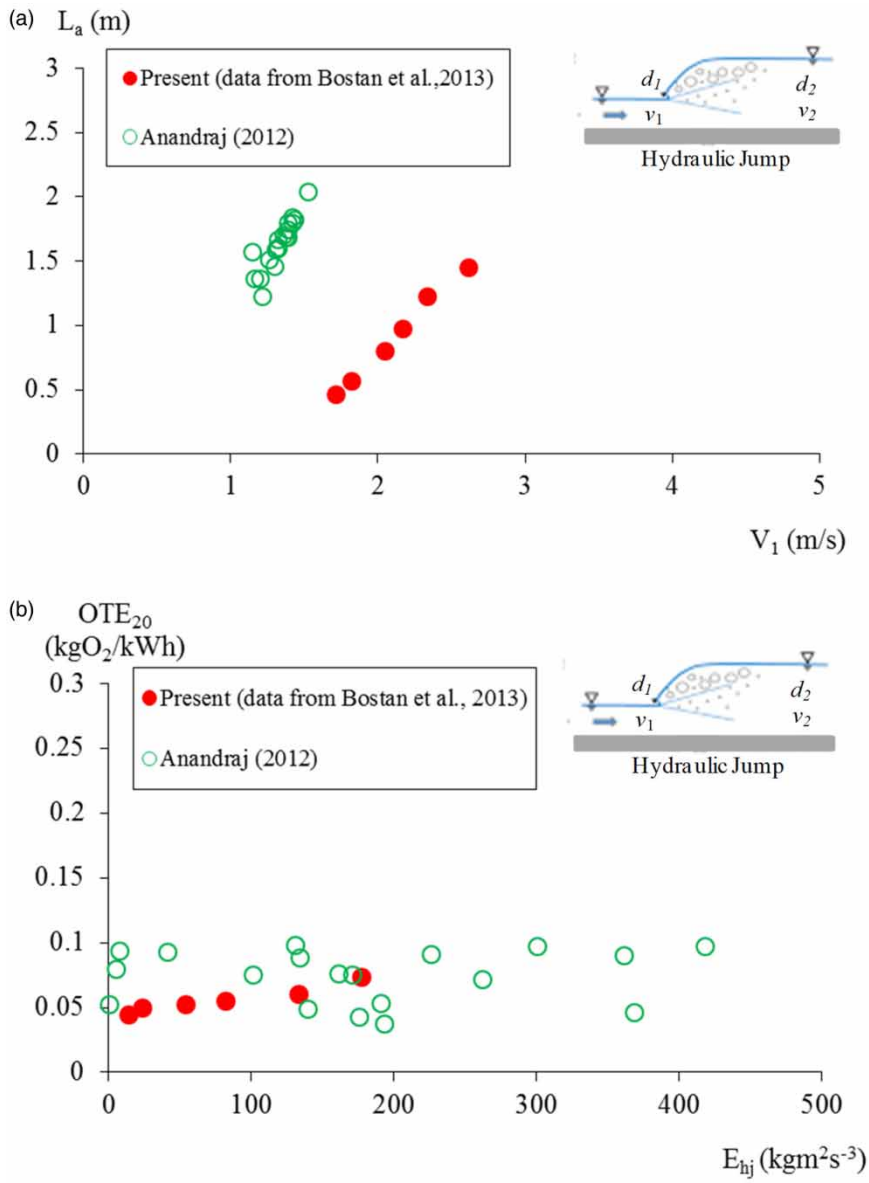

Figure 2 | (a) Aeration length (L_a) in hydraulic jump as a function of jet impact velocity (V_1) and (b) oxygen transfer efficiency (OTE) as a function of energy dissipation rate (E_{hj}).

Gulliver *et al.* (1990) developed the mass transfer equation to calculate OTE for the hydraulic jump in terms of dissolved oxygen at 20 °C and denoted it as OTE_{20}. This can be written as

$$OTE_{20} = 1 - (1 - OTE)^{1/\{1+0.02103(T-20)+8.261 * 10^{-5}(T-20)^2\}} \tag{7a}$$

where OTE_{20} is the OTE at 20 °C and T represents the temperature of the water. Holler (1971) estimated a relationship of OTE for the hydraulic jump as

$$OTE_{20} = 1 - \frac{1}{1 + 0.0463\Delta U^2} \tag{7b}$$

where ΔU represents the velocity difference before and after the hydraulic jump.

Avery & Novak (1978) indicated that one constraint would not be sufficient to express the oxygen transfer efficiency in the hydraulic jump. They said the formulation of OTE_{20} based on the Froude number Fr_1 before the hydraulic jump and Reynolds number R_e, which is given as

$$OTE_{20} = (1 - \frac{1}{k' Fr_1^{2.1} R_e^{0.75}})^{1.115} \tag{7c}$$

where $k^{'}$ is a constant and connected with water salinity concentration. Equation (7a) has been applied to calculate the OTE in the present study.

3.1.4. Energy dissipation rate (E_{hj})

Consider a stationary hydraulic jump as presented in Figure 1(a). The mathematical formulation of the energy dissipation rate for the hydraulic jump is written as

$$E_{hj} = \rho_w g q \Delta H = \rho_w g (V_1 d_1) \frac{(d_2 - d_1)^3}{4 d_2 d_1} \tag{8}$$

where $\Delta H = (d_2 - d_1)^3 / 4 d_2 d_1$ represents the head loss, and it is positive simply if downstream flow depth d_2 is greater than upstream flow depth d_1, which is a necessary condition of the second law of thermodynamics. Furthermore, $q = V_1 d_1$, V_1, and ρ_w denote the water discharge per unit width, the upstream flow velocity, and the water density, respectively. Using Equations (4), (6), and (8) and data of Bostan *et al.* (2013) and Anandraj (2012), we have calculated the OTE and energy dissipation rate, which is plotted in Figure 2(b). The OTE is converted to the standard temperature using Equation (7a). The aeration efficiency is shifted almost parallel to the increased energy loss in Figure 2(b).

3.2. Plunging jets

Once a vertical water jet impacts a receiving pool of water at steady phenomena, entrainment of air bubbles occurs and carries away beneath the free surface of the water's pool. This phenomenon is known as plunging jet air entrainment. A definition sketch and photo of a vertical circular plunging jet are presented in Figure 1(b). According to the literature, the characteristic of air entrainment into water is related to the jet impact velocity. Moreover, observations on vertical plunging jet show that air starts to be entrained when the jet impact velocity exceeds a critical value; see for examples (Biń 1993; Chanson & Cummings 1994; Bertola *et al.* 2018). That is, when the impact velocity is larger than the onset velocity ($V_1 > V_e$), air bubbles are entrained at the impingement point between the supported free-falling jet and the pool of still water. The mechanisms of air bubble entrainment differ depending on the jet impact velocities.

3.2.1. Descriptions of measurement

The measurements of dissolved oxygen were performed by oxygen meter (DO) below the free surface within a cubic type of water pool (50 cm×50 cm×45 cm), and it was constructed with transparent side walls (Figure 3(a)). The plunging water jet was impacted on the free surface of the water in the water pool vertically. The diameter of the circular nozzle was $d_0 =$ 1.3 cm. A high-definition camera was used to take photos of the air entrainment process. The video movies were analysed manually to guarantee the maximum reliability of the data. The camera was positioned beside the plunge pool. Figure 3(a) shows a sketch of the relative positions of the experimental facility and high-speed camera system. The oxygen meter was calibrated before each experiment. The main oxygen electrode was located at the end of the cable. The experiment ranges of DO meter were 0–20 mg/L with the correctness of ± 0.4 mg/L. A digital thermometer with an accuracy of ± 0.1 °C was used for temperature measurements. Before testing the DO the meter was calibrated with signals that simulated the ideal solution (based on a 25 °C ambient environment). DO is best measured directly in the water using a calibrated dissolved oxygen meter. This meter can measure the amount of DO directly in the water as mg/L. Three free falling lengths $x_1 = 30$ cm, $x_1 =$ 20 cm and $x_1 = 10$ cm was investigated for a constant nozzle flow velocity $V_N = 1.51$ m/s.

A visualisation technique was used to determine the penetration depth between the camera and computer. During the experiments, the penetration depths of the entrained air bubbles were constantly more minor than the depth of water in the tank. The water jet impinges onto the water surface vertically, and the jet velocity at an impinging point on the water

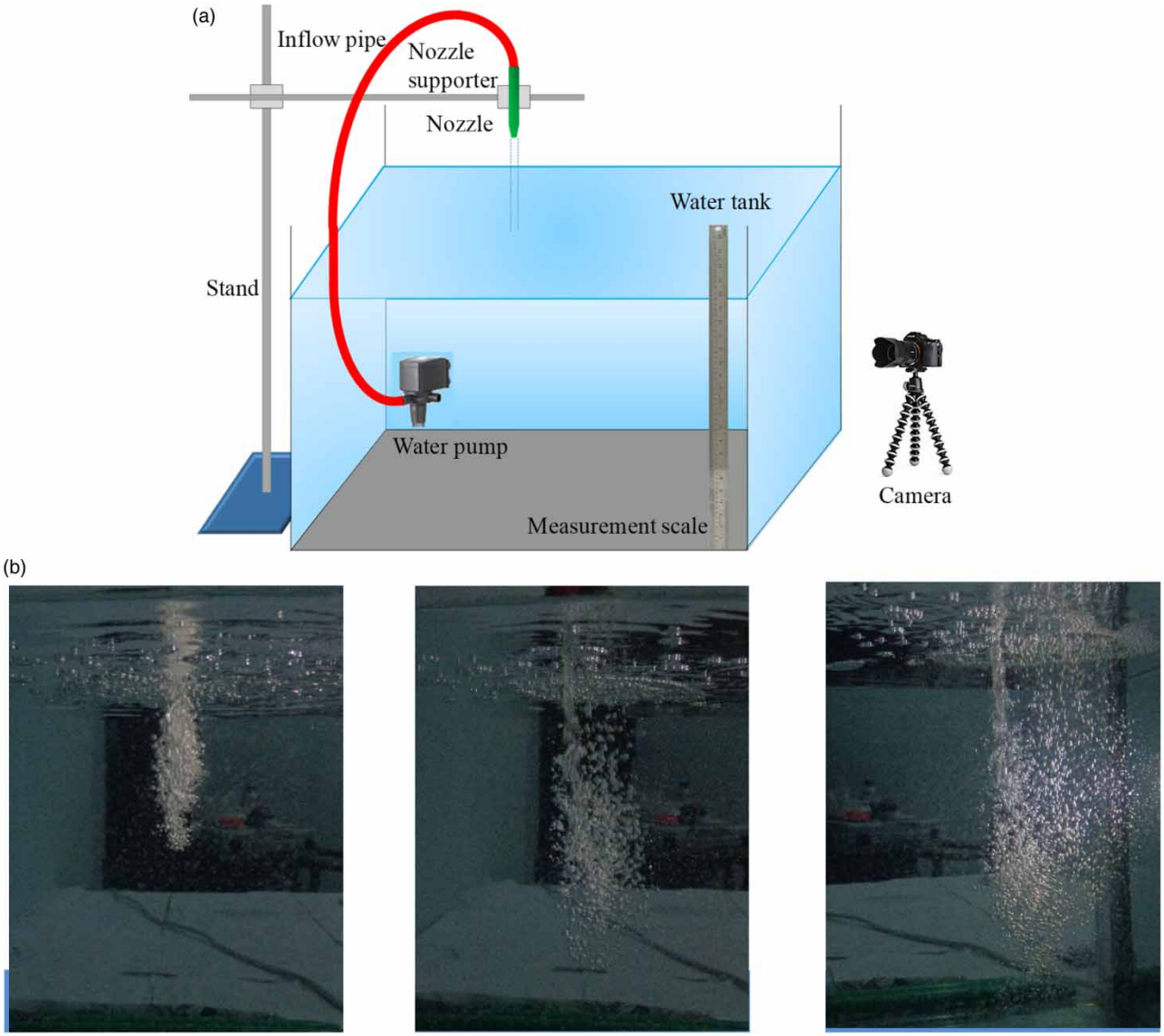

Figure 3 | (a) Schematic diagram of the experimental set-up for vertical plunging water jets and (b) photo of three plumes of bubbles formed by a vertical plunging jet with nozzle velocity $V_N = 1.51$ m/s and several jet lengths.

surface, which the Bernoulli equation can determine as

$$\frac{V_1^2}{2g} = \frac{V_N^2}{2g} + x_1 \tag{9}$$

where $V_1 = \sqrt{V_N^2 + 2gx_1}$ is the jet velocity at the impinging point, V_N represents the nozzle velocity of water, and x_1 denotes the free-falling water length.

3.2.2. Penetration depth (P_d)

The penetration depth is defined as the depth between the free surface and the point where the rising velocity of the bubble equals the vertical water speed. Several researchers measured the penetration depth in the vertical circular plunging jets system (Kumagai & Endoh 1983; Ohkawa *et al.* 1987; Harby *et al.* 2014). In the present study, Figure 3(b) shows the three representative bubble swarm images for jets with three different free-falling lengths $x_1 = 30$ cm, $x_1 = 20$ cm, and $x_1 = 10$ cm with the same nozzle flow velocity of $V_N = 1.51$ m/s, respectively. The penetration depths were determined

vertically from impinging point to a stable point by a video camera. The lower part of the bubble cloud constantly oscillates with time (the lower part was not fully stable), so the time-averaged penetration depth was determined. It is seen in Figure 3(b) that the jet with the higher free-falling length causes more bubble entrainments and lower penetration depth (P_d). Furthermore, we can see that the penetration depth is decreased with the increase of jet impact velocity in Figure 4(a), which follows the results of Qu *et al.* (2011) and Hoque (2002). Penetration depth, $P_{d,}$ is dependent on x_1, V_N/d_N and the nozzle aspect ratio l_N/d_N (see Kumagai & Endoh 1983; Ohkawa *et al.* 1987).

3.2.3. Oxygen transfer efficiency

The oxygen transfer performance of vertical plunging jets is usually uttered based on standard oxygen transfer rate (O_RV), which can be obtained as

$$OTE_{20} = \frac{O_R V}{E_{pj}} \tag{10}$$

where O_R represents the rate of oxygen transfer (mg/L/h) at 20 °C and 1 atm pressure, V represents the aerated volume of water (m^3), and E_{pj} is an upstream energy transport rate (J/(m.s)). The mathematical definition of O_R is given as below

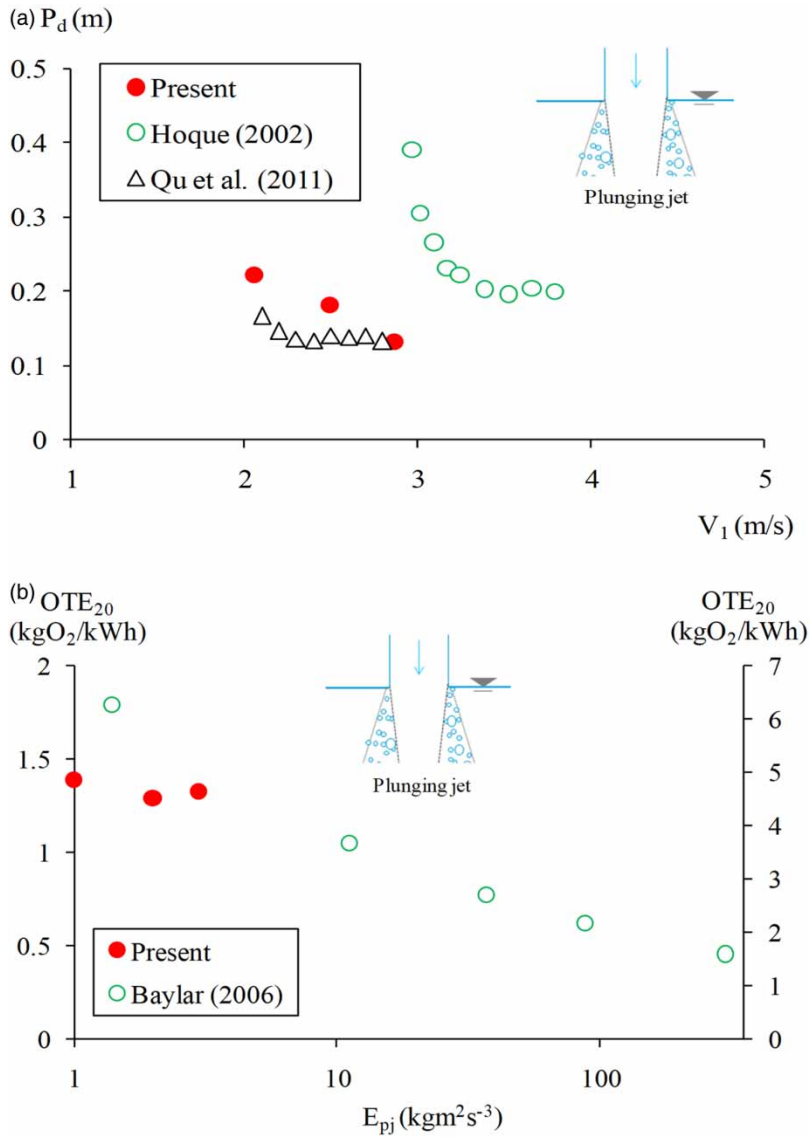

Figure 4 | (a) Relationship between penetration depth (P_d) and jet impact velocity (V_1) and (b) variation of oxygen transfer efficiency (OTE) with the energy dissipation rate (E_{pj}).

(Deswal & Verma 2007):

$$O_R = K_L a \times 3600 \times C_s^* \tag{11}$$

where C_S^* is the saturation dissolved oxygen concentration in water at standard conditions (mg/L).

In the case of a plunging jet, laboratory experiments were conducted to determine the oxygen transfer efficiency (*OTE*). From a typical sample of the deoxygenated water, C_0 was measured initially. After aeration, a certain period ($t = 5$ minutes), samples of oxygenated water were taken to calculate oxygen concentration (C_t) after time t. Finally, the values of $K_L a$, O_R, and OTE_{20} were computed using Equations (4), (11) and (10), respectively.

3.2.4. Upstream energy transport rate (E_{pj})

Mathematically, the upstream energy transfer rate for a vertical circular plunging jet is defined as

$$E_{pj} = \frac{1}{2}\rho_w Q_w V_1^2 = \frac{\pi}{2}\rho_w V_1^3 r_1^2 \tag{12}$$

where r_1 is the radius of the water jet (m) at the impinging point, and Q_w denotes the water discharge or water jet flow rate (m^3/s). The results regarding aeration efficiency in vertical circular plunging jets are presented in section 4.

3.3. Plunging breaking waves

An air entrainment phenomenon occurs at plunging breaking waves which contribute to the oxygen transfer through an air-water interface. At the impact point, Chanson & Lee (1997) showed similarities between plunging jet and plunging breakers (deeper waters). The jet impact velocity may be scaled by $2gH_{b,}$ where the water jet thickness is approximately $0.05{*}H_b$. The aeration characteristics and penetration depth of plunging breaking waves in the sea have similarity with the plunging jets which occurs in the waterfall (Koga 1982; Chanson & Cummings 1992). The relationship of air entrainment between plunging waves and jets is reinvestigated through such evidence.

3.3.1. Data collection

DO is a vital water parameter that was measured by a Senso Direct DO meter (Figure 5(a)). The measurement ranges of the oxygen meter were 0–20 mg/L for DO with an accuracy of ± 0.4 mg/L and 0–50 °C for temperature with an accuracy of ± 0.8 °C. Before testing the DO, the meter was calibrated with signals that simulated the 'ideal' solution (based on a 25 °C ambient environment). The sampling region of this study is the coastal area of the southeastern part of Bangladesh near the Cox's Bazar, which lies between 21° 11′ 6″ N latitude and 92° 2′ 52.8″ E longitude. In Figure 5(a), points A to E show the sampling points for the air-water mixture. The sampling implies A, B, C, D and E were fixed with a distance of 1.5 m at the inner surf zone. The data were collected from the mentioning points, analysed by the Gas Analyzer meter. For each sample, measurements of DO were taken by immersing the electrode probe and are plotted in Figure 5(c).

Tsoukala & Moutzouris (1996) presented experimental data of oxygen transfer for breaking waves. In their experiment, the beach slope of l:2.3 was positioned at the end of the wave flume, and water depth and wave period were considered 72 cm and 1.55 s, respectively. Wave frequencies with ranges of 0.65–0.90 Hz and wave heights in the ranges of 8.5–20.5 cm were generated. Characteristically, the generated waves were plunging breaker types. The dissolved oxygen in the air-water mixture was measured over time by a handy DO meter brand OXI-96 at 21 examining locations through the flume. The transfer coefficients K_L were determined from the wave breaking area at 20 °C.

3.3.2. Penetration depth (P_d)

In the surf zone, the penetration depth (P_d) of air bubbles for plunging breaking waves is found as the depth between the free surface of the water and the deepest air entrainment point, where the air bubbles are reached during the wave breaking process (Figure 1(c)). Significant fluid turbulence occurs where breaking waves completely disintegrate after their crest impinges against water. At this impinge point, the downward velocity of air bubbles turns to zero, where the buoyancy force works against these. The driven air bubbles are broken into tiny bubbles by buoyancy force, and these air bubbles rise to the free surface. During their experiments, the penetration depths were recorded and determined vertically from the impinging point to a stable point by Chanson & Lee (1997). Their results recommended that the bubbles were entrained downward up to 1.2–2 times the wave amplitude beneath the free surface.

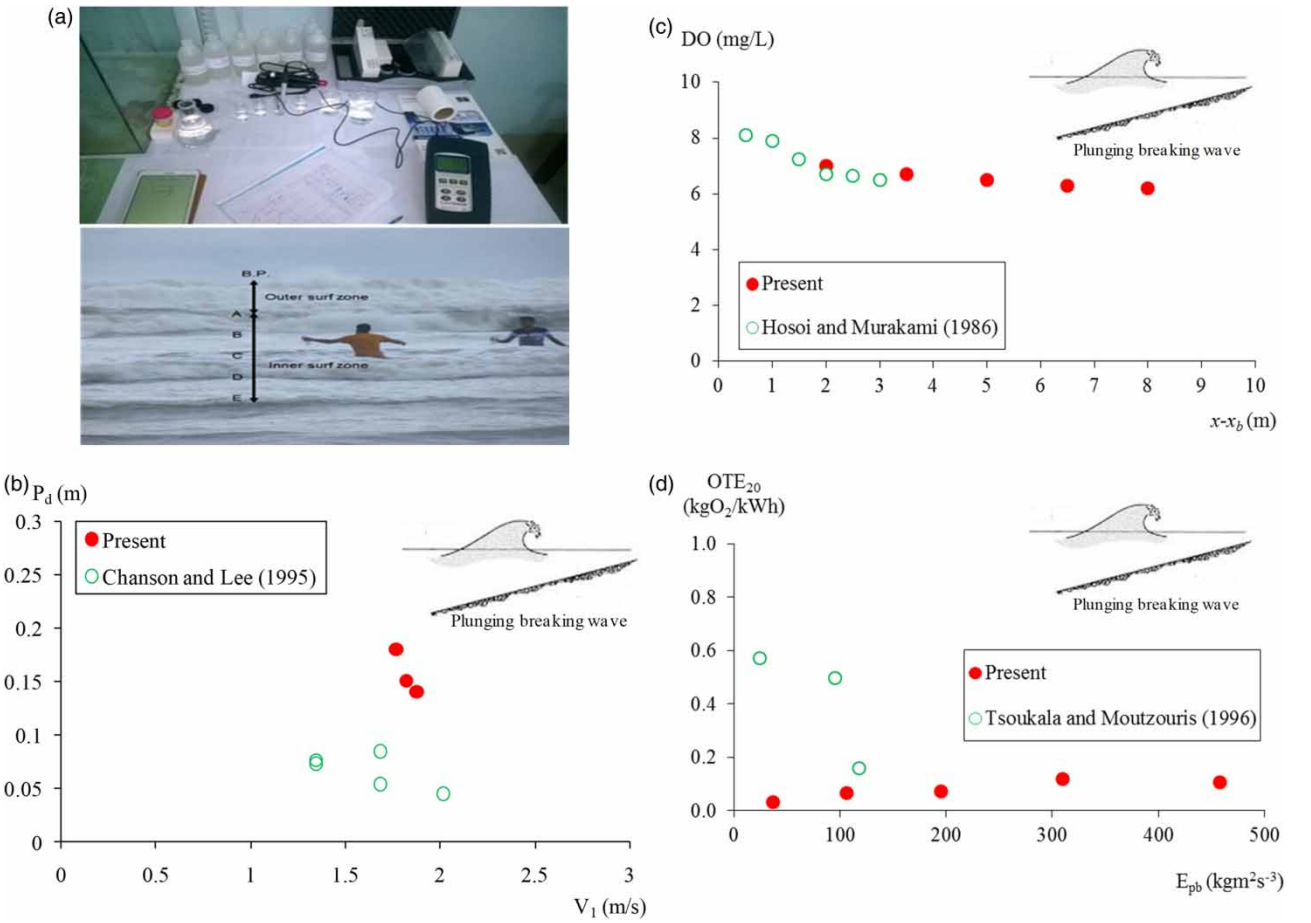

Figure 5 | (a) Photo of gas exchange instruments, (b) penetration depth (P_d) in a plunging breaker as a function of jet impact velocity (V_1), (c) variation of dissolved oxygen concentration (*DO*) against the onshore distance, and (d) comparison of oxygen transfer efficiency (*OTE*) versus energy dissipation rate (E_{pb}).

3.3.3. Oxygen transfer efficiency

Applying a similar calculation method as the hydraulic jump, OTE is calculated using Equation (6), knowing the gas transfer coefficient from Tsoukala & Moutzouris (1996). They measured the transfer coefficients K_L from the breaking area, and after that, it transformed to 20 °C using Equation (13), which was derived by Daniil & Gulliver (1988):

$$OTE_{20} = 1 - \exp(K_L a t) \tag{13}$$

3.3.4. Energy transport rate (E_{pb})

The wave energy transmitted by the water wave motion from the deepwater toward the shore is written by

$$E_{pb} = (1/8)\rho_w g H_0^2 c_g = \rho_w g^2 H_0^2 T/(32\pi) \tag{14}$$

where c_g, H_0, and T represent the group velocity, deepwater wave height, and wave period, respectively. If we assume that the total energy is dissipated by the progressive wave in the surf zone, we can write

$$E_{pb} = g^2 H_0^2 T/(32\pi V_b) \tag{15}$$

where V_b denotes the water volume per unit width.

Introducing $V_b = \frac{h_b^2}{2i}$, the above equation can be rewritten as

$$E_{pb} = ig^2 H_0^2 T/(16\pi h_b^2) \tag{16}$$

where i is the beach slope.

4. RESULTS AND DISCUSSION

The similarity of aeration efficiency, DO, and penetration depth among the hydraulic jumps, plunging jets, and plunging breaking waves are investigated and plotted against the energy loss and jet impact velocity. In Figure 2(a), the aeration length increases with jet impact velocity. The resulting trend in Figure 2(a) is similar to Anandraj (2012) data. Bostan *et al.* (2013) and Hager *et al.* (1990) measured the aeration length for a hydraulic jump, and they found that it was increased with the jet impact velocity.

On the other hand, Figure 2(b) shows the OTE for a hydraulic jump, which is presented against the energy dissipation rate. It is seen in Figure 2(b) that with the increase of energy dissipation rate in a hydraulic jump, OTE is almost parallel shifted, which is consistent with the result of Anandraj (2012). As Kucukali & Cokgor (2009) mentioned, OTE increased with the increase of energy dissipation along with the jump. This may be because the saturation values of DO and initial DO values of water influence the aeration process. Liu *et al.* (2004) demonstrated the direct relationship between head loss and turbulence kinetic energy. Ozkan *et al.* (2014) measured the aeration efficiency related to the air-demand ratio and Froude number.

The penetration depth of air bubbles created by plunging water jet, P_d, and the OTE results (OTE) is plotted in Figure 4, which are varied with the jet impact velocity V_1 and energy dissipation rate E_{pj}, respectively. Figure 4(a) shows the changes in penetration depths, P_d formed by the water jets. It is observed from Figure 4(a) that P_d decreases with the increasing V_1 for a particular value of V_N. Hoque (2002), Qu *et al.* (2011) and Harby *et al.* (2014) also measured the penetration depth against the jet impact velocity, and they found similar results to those that are plotted in Figure 4(a). Cumming (1975) showed theoretically that the penetration depth was linked to the jet velocity. In addition, the oxygen transfer performance of the vertical circular plunging jets was calculated using Equation (10). As shown in Figure 4(b), the measured results of oxygen transfer efficiency are found reasonably consistent with the data of Baylar *et al.* (2006), although present obtained data are very scarce.

We have also investigated the gas exchange phenomena by plunging breaking waves in the coastal area. As displayed in Figure 5(b), the penetration depth decreases with the increase of plunging breaking jet velocity, which has similarities with the plunging jet. Moreover, it is found that DO is reduced with the increase of a shoreward distance in Figure 5(c). After the breaking point, many bubbles are entrained into the water, producing greater oxygen absorption. Similar results were measured by Hosoi & Murakami (1986). In Figure 5(d), we have also observed that OTE almost keeps constant with the increase of energy dissipation rate for the present study; those are calculated using Equations (13) and (14).

Free surface flows are typically scaled with the Froude similitude keeping identical Fr_1 both in the model and prototype. Usually, the selection of the Froude similitude is derived based upon some primary theoretical considerations and air transport in models are affected by the scale effect. In this study, the comparative analysis of OTE, which is calculated based on the oxygenation for hydraulic jumps, has revealed almost identical for $Fr_1 = 2.5$–4.0 (Figure 2(b)). New air-water flows properties were measured in vertical circular plunging jets. The data set together with the earlier data of Baylar *et al.* (2006) yielded scale effects in terms of oxygenation (Figure 4(b)) with identical inflow Froude numbers ($Fr_1 = 8.0$–13.0). The scale effects also affected the oxygenation process by air bubbles in the surf zone and laboratory wave flume (Figure 5(d)). The entrained air bubbles or DO are not similar to the large-scale physical models compared to laboratory wave flumes.

5. CONCLUSIONS

The analogies of gas exchange among hydraulic jumps, plunging jets, and plunging waves may be appropriate to work out quantities under modelling efforts. The obtained results from the data analysis can be summarised as below:

(1) The length of aeration in hydraulic jumps and penetration depths both in plunging jets and plunging breakers were found to be pretty similar, and those were dependent on the jet impact velocity.

(2) OTE was shifted almost parallel with the increased energy loss in the case of hydraulic jumps. On the other hand, it was found that the OTE is attenuated as the increased energy dissipation rate in plunging jets and it kept constant in plunging breaking waves. Further research work is necessary in this regard.
(3) A scale effect was observed in terms of the oxygenation for identical inflow conditions of a vertical circular plunging jet, whereas it was similar for the hydraulic jump. Furthermore, the scale effect was found distinct between the small-scale laboratory results and field conditions.
(4) These investigations and observations might provide valuable evidence for evaluating the oxygen transfer rate and ocean aeration due to spilling and plunging breakers.

CONFLICTS OF INTEREST

The authors declare no conflicts of interest regarding the publication of this paper.

FUNDING

The authors received no research grants or funding from any funding agencies to perform this study.

DATA AVAILABILITY STATEMENT

All relevant data are included in the paper or its Supplementary Information.

REFERENCES

Alekseyev, V. & Kokorin, A. 1984 The effect of bubbles formed by breaking wind waves on air-sea gas transfer. *Atmospheric Ocean Physics* **20** (7), 554–559.
Anandraj, A. 2012 Investigational study on self-aeration characteristic of hydraulic jump. *IOSR Journal of Mechanical Civil Engineering (IOSR-JMCE)* **4** (2), 27–31.
Arora, S. & Keshari, A. K. 2021 Dissolved oxygen modeling of Yamuna River using different ANFIS models. *Water Science & Technology* **0** (1), 466.
Avery, S. T. & Novak, P. 1978 Oxygen transfer at hydraulic structures. *Journal of the Hydraulics Division* **104** (11), 1521–1540.
Baylar, A., Emiroglu, M. E. & Ozturk, M. 2006 The development of aeration performance with different typed nozzles in a vertical plunging water jet system. *International Journal of Science & Technology* **1** (1), 51–63.
Bertola, N., Wang, H. & Chanson, H. 2018 A physical study of air–water flow in planar plunging water jet with large inflow distance. *International Journal of Multiphase Flow* **100**, 155–171.
Biń, A. K. 1993 Gas entrainment by plunging liquid jets. *Chemical Engineering Science* **48** (21), 3585–3630.
Bostan, T., Coşar, A., Yetilmezsoy, K., Topçu, S. & Ağaççıoğlu, H. 2013 The effect of hydraulic jump on the aeration efficiency. In *Proceeding of BCCCE*. Epoka University, Albania.
Chanson, H. 1995 Air-water gas transfer at hydraulic jump with partially developed inflow. *Water Research* **29** (10), 2247–2254.
Chanson, H. & Cummings, P. D. 1992 *Aeration of the Ocean due to Plunging Breaking Waves*. Research Report No. CE142. Dept. of Civil Eng., University of Queensland. p. 42.
Chanson, H. & Cummings, P. D. 1994 Effects of plunging breakers on the gas contents in the oceans. *Marine Technology Society Journal* **28** (3), 22–32.
Chanson, H. & Lee, J. F. 1997 Plunging jet characteristics of plunging breakers. *Coastal Engineering* **31** (1–4), 125–141.
Cihat Tuna, M., Ozkan, F. & Baylar, A. 2014 Experimental investigations of aeration efficiency in high-head gated circular conduits. *Water Science and Technology* **69** (6), 1275–1281.
Cumming, I. W. 1975 *The Impact of Failing Liquids with Liquid Surfaces*. *PhD Thesis*.
Daniil, E. I. & Gulliver, J. S. 1988 Temperature dependence of liquid film coefficient for gas transfer. *Journal of Environmental Engineering* **114** (5), 1224–1229.
Deswal, S. & Verma, D. V. S. 2007 Air-water oxygen transfer with multiple plunging jets. *Water Quality Research Journal* **42** (4), 295–302.
Estrella, J., Wüthrich, D. & Chanson, H. 2021 Two-phase air-water flows in hydraulic jumps at low Froude number: similarity, scale effects and the need for field observations. *Experimental Thermal and Fluid Science* **130**, 110486.
Gameson, A. L. H. 1957 Weirs and the aeration of rivers. *Journal of the Institution of Water Engineers* **11**, 477–490.
Gulliver, J. S., Thene, J. R. & Rindels, A. J. 1990 Indexing gas transfer in self-aerated flows. *Journal of Environmental Engineering* **116** (3), 503–523.
Guyot, G., Cartellier, A. & Matas, J. P. 2020 Penetration depth of a plunging jet: from microjets to cascades. *Physical Review Letters* **124** (19), 194503.
Hager, W. H., Bremen, R. & Kawagoshi, N. 1990 Classical hydraulic jump: length of roller. *Journal of Hydraulic Research* **28** (5), 591–608.
Harby, K., Chiva, S. & Muñoz-Cobo, J. L. 2014 An experimental study on bubble entrainment and flow characteristics of vertical plunging water jets. *Experimental Thermal and Fluid Science* **57**, 207–220.

Holler, A. G. 1971 The mechanism describing oxygen transfer from the atmosphere to discharge through hydraulic structures. In *Proc. IAHR*. Vol. 45, pp. 373–382.

Hoque, A. 2002 *Air Bubble Entrainment by Breaking Waves and Associated Energy Dissipation*. Toyohashi University of Technology, Japan, p. 151.

Hosoi, Y. & Murakami, H. 1986 Effect of breaking waves on dissolved oxygen and organic matter. *Coastal Engineering Proceedings* **1** (20), 2498–2512.

Hosoi, Y., Murakami, H. & Oto, M. 1984 Reaeration by spilling breaker. *Coastal Engineering in Japan* **27** (1), 97–108.

Iguchi, M., Okita, K. & Yamamoto, F. 1998 Mean velocity and turbulence characteristics of water flow in the bubble dispersion region induced by plunging water jet. *International Journal of Multiphase Flow* **24** (4), 523–537.

Jadhav, S. S., Shinde, S. D. & Zubair, S. M. 2017 Regulator of hydraulic jump by providing rise in bed. *International Journal of Science Technology and Management* **6** (4), 22–29.

Kamal, R., Zhu, D. Z., Crossman, J. A. & Leake, A. 2020 Case study of total dissolved gas transfer and degasification in a prototype ski-jump spillway. *Journal of Hydraulic Engineering* **146** (9), 05020007.

Koga, M. 1982 Bubble entrainment in breaking wind waves. *Tellus* **34** (5), 481–489.

Kucukali, S. & Cokgor, S. 2009 Energy concept for predicting hydraulic jump aeration efficiency. *Journal of Environmental Engineering* **135** (2), 105–107.

Kumagai, M. & Endoh, K. 1983 A note on the relationship between gas entrainment curve and its starting velocity. *Journal of Chemical Engineering of Japan* **16** (1), 74–75.

Kumar, M., Ranjan, S. & Tiwari, N. K. 2018 Oxygen transfer study and modeling of plunging hollow jets. *Applied Water Science* **8** (5), 1–15.

Leng, X. & Chanson, H. 2019 Air-water interaction and characteristics in breaking bores. *International Journal of Multiphase Flow* **120**, 103101.

Liu, M., Rajaratnam, N. & Zhu, D. Z. 2004 Turbulence structure of hydraulic jumps of low Froude numbers. *Journal of Hydraulic Engineering* **130** (6), 511–520.

McKeogh, E. J. & Ervine, D. A. 1981 Air entrainment rate and diffusion pattern of plunging liquid jets. *Chemical Engineering Science* **36** (7), 1161–1172.

Miller, R. L. 1987 Role of vortices in surf zone prediction: sedimentation and wave forces. In: *Beach and Nearshore Sedimentation: based on a symposium sponsored by the Society of Economic Paleontologists and Mineralogists*, eds. Davis, R. A., Jr., & Ethington, R. L., Tulsa, Oklahoma, USA, pp. 92–114.

Montano, L. & Felder, S. 2020 An experimental study of air–water flows in hydraulic jumps on flat slopes. *Journal of Hydraulic Research* **58** (5), 767–777.

Ohkawa, A., Kusabiraki, D. & Sakai, N. 1987 Effect of nozzle length on gas entrapment characteristics of vertical liquid jet. *Journal of Chemical Engineering of Japan* **20** (3), 295–300.

Ohl, C. D., Oguz, H. N. & Prosperetti, A. 2000 Mechanism of air entrainment by a disturbed liquid jet. *Physics of Fluids* **12** (7), 1710–1714.

Ozkan, F., Tuna, M. C., Baylar, A. & Ozturk, M. 2014 Optimum air-demand ratio for maximum aeration efficiency in high-head gated circular conduits. *Water Science and Technology* **70** (5), 871–877.

Qu, X. L., Khezzar, L., Danciu, D., Labois, M. & Lakehal, D. 2011 Characterization of plunging liquid jets: a combined experimental and numerical investigation. *International Journal of Multiphase Flow* **37** (7), 722–731.

Rajaratnam, N. 1967 Hydraulic jumps. In: *Advances in Hydroscience*, Vol. 4 (V. Te Chow, ed.). University of Edmonton, Elsevier, pp. 197–280.

Retsinis, E. & Papanicolaou, P. 2020 Numerical and experimental study of classical hydraulic jump. *Water* **12** (6), 1766.

Saleem, M. R., Ali, I. & Qamar, S. 2018 Application of discontinuous Galerkin method for solving a compressible five-equation two-phase flow model. *Results in Physics* **8**, 379–390.

Sarmiento, J. L., Orr, J. C. & Siegenthaler, U. 1992 A perturbation simulation of CO_2 uptake in an ocean general circulation model. *Journal of Geophysical Research: Oceans* **97** (C3), 3621–3645.

Suciu, G. D. & Smigelschi, O. 1976 Size of the submerged biphasic region in plunging jet systems. *Chemical Engineering Science* **31** (12), 1217–1220.

Tans, P. P., Fung, I. Y. & Takahashi, T. 1990 Observational contrains on the global atmospheric CO_2 budget. *Science* **247** (4949), 1431–1438.

Tiwari, N. K. 2021 Evaluating hydraulic jump oxygen aeration by experimental observations and data driven techniques. *ISH Journal of Hydraulic Engineering*, **27**, 1–15.

Tsoukala, V. K. & Moutzouris, C. I. 1996 Scale effects in oxygenation in the breaker zone of coastal structures. *Coastal Engineering* **25**, 403–414.

Van de Sande, E. & Smith, J. M. 1976 Jet break-up and air entrainment by low velocity turbulent water jets. *Chemical Engineering Science* **31** (3), 219–224.

Wallace, D. W. R. & Wirick, C. D. 1992 Large air–sea gas fluxes associated with breaking waves. *Nature* **356** (6371), 694–696.

Witt, A. M. & Gulliver, J. S. 2012 Predicting oxygen transfer efficiency at low-head gated sill structures. *Journal of Hydraulic Research* **50** (5), 521–531.

Wüthrich, D., Shi, R. & Chanson, H. 2020 Physical study of the 3-dimensional characteristics and free-surface properties of a breaking roller in bores and surges. *Experimental Thermal and Fluid Science* **112**, 109980.

Yang, M., Smyth, T. J., Kitidis, V., Brown, I. J., Wohl, C., Yelland, M. J. & Bell, T. G. 2021 Natural variability in air–sea gas transfer efficiency of CO2. *Scientific Reports* **11**, 13584.

First received 17 November 2021; accepted in revised form 31 January 2022. Available online 15 February 2022